J Nanopart Res (2019) 21: 113
https://doi.org/10.1007/s11051-019-4540-3

RESEARCH PAPER

# Carbon nanotubes/SiC prepared by catalytic chemical vapor deposition as scaffold for improved lithium-sulfur batteries

**Jiayi Wang · Wenjuan Wang · Haipeng Li · Taizhe Tan · Xin Wang · Yan Zhao**

Received: 30 January 2019 / Accepted: 25 April 2019 / Published online: 28 May 2019


**Abstract** The low conductivity of sulfur and shuttle effect of lithium polysulfides have limited the applications of Li-S batteries. In this account, carbon nanotubes/SiC (CNTs/SiC) composites were prepared by means of catalytic chemical vapor deposition (CCVD). SiC was used as the matrix for growth of CNTs and ferrocene served as catalyst. The surface of SiC was successfully loaded with carbon nanotubes, which underwent increasing growth to form clusters. Sulfur was added into CNTs/SiC by the hydrothermal method to yield sulfur-carbon nanotubes/SiC composites (S-CNTs/SiC) for Li-S batteries. SiC was strongly bound to lithium polysulfides (LPS) through chemical interactions and CNTs attracted LPS by physical absorption. CNTs provided good electrical conductivity for the overall composite and SiC enhanced adsorption ability of LPS. DFT calculation was carried out to illustrate direct Si-S interaction and strong confinement on LPS of SiC. Both factors synergistically reduced loss in active substances during battery cycling. The resulting S-CNTs/SiC electrodes displayed discharge capacity of 685 mAh $g^{-1}$ at 0.1 C after 100 cycles, coupled with excellent cycle performance of 316 mAh $g^{-1}$ after 400 cycles at 1 C.

**Keywords** Carbon nanotubes · SiC · Li-S batteries · Electrochemical performance · Modeling and simulation · Energy storage

J. Wang · W. Wang · H. Li (✉) · Y. Zhao (✉)
School of Materials Science and Engineering, Hebei University of Technology, Tianjin 300130, China
e-mail: lihp_hebut@outlook.com
e-mail: yanzhao1984@hebut.edu.cn

T. Tan
Synergy Innovation Institute of GDUT, Heyuan, Guangdong Province, China

X. Wang
International Academy of Optoelectronics at Zhaoqing, South China Normal University, Guangzhou, Guangdong Province, China

## Introduction

The development of sophisticated modern technologies requires advanced rechargeable lithium batteries with high energy densities and good cycle performances (He et al. 2017a; Zhou et al. 2015; He et al. 2016a; He et al. 2018c) Lithium-sulfur batteries (LSBs) have drawn great attention owing to their high theoretical capacities (1675 mAh $g^{-1}$) and abundant reserves of sulfur (Zhang et al. 2014a; He et al. 2019; Bruce et al. 2012; He et al. 2018a; Zhang et al. 2014b; He et al. 2018b) However, some problems impede the industrialization of LSBs. First, pure sulfur is insulator with electrical conductivity of $5 \times 10^{-30}$ S $cm^{-1}$ at room temperature, making electrons and ions transfer difficultly. Second, the intermediate products of sulfur called lithium polysulfides (LPS) could easily dissolve in electrolyte solutions, decreasing the electroactive substances. Third, the density of sulfur is different from that of final product ($Li_2S$), resulting in large volume expansions (~ 80%) (Miao et al. 2013; He et al. 2017b;

Mikhaylik and Akridge 2004; He et al. 2016b; Zhang et al. 2013; Ji et al. 2009; Yin et al. 2017; He et al. 2015). To overcome these problems, current methods mainly focused on the modification of cathode materials by adsorption (Hong et al. 2019) and coating (Li et al. 2014). The modification of cathode materials with coated carbon, conductive polymers (Wei et al. 2015), and oxides (Wang et al. 2014) could be very effective in slowing down the shuttle effect of LSBs. This, in turn, would enhance the use of active substances and improve the electrochemical performances of LSBs.

Among these, carbon-based materials, such as CNTs (Xiang et al. 2017), porous carbon (Wang et al. 2018), and graphene (Huang et al. 2013), could be prepared by simple route to yield stable substances. Hence, they are widely utilized in LSBs. For instance, Zhao et al. reported novel tube-in-tube structured carbon nanomaterials for LSBs with high discharge capacities reaching 918 mAh $g^{-1}$ at 500 mA $g^{-1}$ after 50 cycles (Zhao et al. 2014). Bao et al. prepared hierarchical structure of graphite oxide@mesoporous carbon for LSBs with great reversible capacities and excellent cycle abilities (Bao et al. 2014). However, polysulfides are often trapped by weak physical absorption in carbon materials, and tremendous efforts have been devoted for promoting adsorption of polysulfides (Li et al. 2016a; Wu et al. 2018; Evers et al. 2012). Some recent studies displayed that strong affinity to $S_8$ and polysulfides can be caused by direct Si–S and Li–C interaction (Li and Zhao 2018). Therefore, our attention was focused on SiC as stable compound in terms of thermodynamics, chemistry, and physics. SiC is often considered as inert component when used in batteries. Besides, recent studies have confirmed its relevant electrochemical activity (Hu et al. 2016; Li et al. 2016b).

In this study, carbon nanotubes/SiC (CNTs/SiC) were prepared through CCVD and used for loading of sulfur. The carbon nanotubes were grown on SiC matrix. This unique structure could effectively adsorb polysulfides and reduce loss in active substances, enhancing the conductivity of electrodes and greatly preventing volume expansion. The obtained S-CNTs/SiC composite with 75.6 wt% sulfur content showed great cycling performances and excellent rate capabilities as cathode material of LSBs. Discharge capacities reaching 685 mAh $g^{-1}$ after 100 cycles at 0.1 C were obtained.

## Experimental

### Synthesis of CNTs/SiC

First, SiC (≤ 5 μm, 100 g) was placed in 500 mL of 20% HF solution and stirred for 24 h to remove $SiO_2$ layers deposited SiC surface. The sample was then washed several times with deionized water to keep the pH around 7. Subsequently, SiC was evenly spread at bottom of the porcelain boat employed as growth matrix of CNTs. The porcelain boat was then placed in a tube furnace heated to 600 °C under argon atmosphere (99.9% purity, 500 mL/min). Second, 1 g ferrocene dissolved in 20 mL xylene was used as Fe catalyst. The catalyst was injected into the tube furnace at a rate of 0.2 mL/min for 20 min using a syringe system. Meanwhile, argon (500 mL/min), hydrogen (50 mL/min), and acetylene (5 mL/min) were fed into the tube furnace for 20 min. Subsequently, the furnace was cooled down to room temperature under argon (450 mL/min).

### Synthesis of S-CNTs/SiC

CNTs/SiC and sulfur powder at ratio of 1:4 were ground uniformly, then placed in a stainless steel vessel under argon atmosphere, and kept at 155 °C for 12 h to prepare S-CNTs/SiC.

### Characterization methods

The X-ray diffraction (XRD) patterns were collected on a Bruker D8 Discover machine using Cu-K$\alpha$ radiation ($\lambda = 0.154056$ nm) at two-theta ranging from 10° to 90° and scan rate of 12°/min. The content of sulfur was evaluated by thermal gravimetry analysis (TGA, NETZSCH STA-409PC) at 30–800 °C under argon flow at heating rate of 5 °C/min. The Hitachi S-4800 equipment was used to capture the scanning electron microscopy (SEM) images. Transmission electron microscopy (TEM, JEOL 2100) was utilized for material morphology and structure determination. The Raman spectra were recorded on Horiba-Jobin-Yvon LabRAM HR800 Raman Spectrometer. Micrometritics ASAP 2020 analyzer was employed to analyze the nitrogen adsorption and desorption isotherms. The surface functional groups of S-CNTs/SiC were characterized by X-ray photoelectron spectroscopy (XPS, Thermo Scientific K-Alpha XPS). The specific surface and pore size

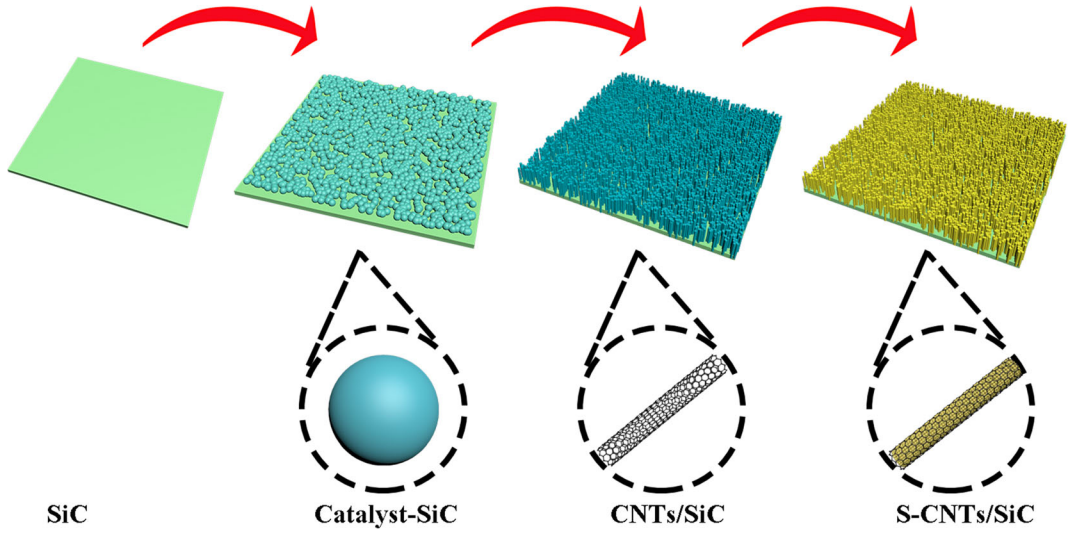


**Fig. 1** Synthetic route of S-CNTs/SiC composites

distribution of the samples were conducted by Brunauer-Emmett-Teller (BET, V-Sorb 2800P).

## Electrochemical measurements

A mixture of 80 wt% S-CNTs/SiC composites, 10 wt% Super P, and 10 wt% PVDF was first dissolved in NMP. The mixture was then coated on carbon-coated aluminum foil by doctor blade, keeping sulfur loading of around 2 mg $cm^{-2}$. The modified aluminum was then punched to form 9-mm diameter circular disks. The electrochemical measurements of S-CNTs/SiC composites were performed in button cells (2025 type) using S-CNTs/SiC composites cathode and lithium foil counter electrode. The button cells were assembled in a glovebox filled with argon (99.9%) using Celgard 2400 as separator. The electrolyte was composed of 1 M lithium bis (trifluoromethanesulfonyl) imide (LiTFSI) dissolved in 1,3-dioxolane and dimethoxymethane ($v/v = 1:1$) with 1 wt% of $LiNO_3$. The cyclic voltammograms (CV) were obtained on a Princeton VersaSTAT 4 potentiostat at 0.1 mV $s^{-1}$. The galvanostatic discharge-charge tests were analyzed using a Neware battery tester at 1.5–3.0 V.

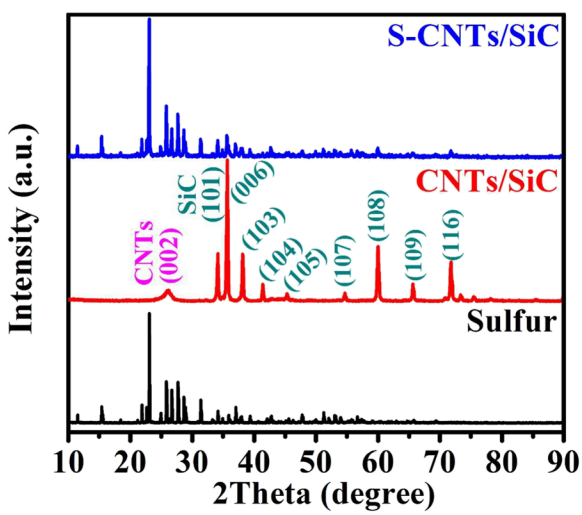


**Fig. 2** XRD patterns of sulfur, CNTs/SiC, and S-CNTs/SiC

## Theoretical calculations

Density functional theory (DFT) calculation was conducted by the Vienna Ab initio Simulation Package (VASP). Perdew-Burke-Ernzerhof version of generalized gradient approximation was employed to characterize the exchange correlation functional and the plane wave was set as 400 eV. Monkhorst-Pack grid of 2 × 2 × 1 was adopted with a vacuum distance of 15 Å. During the calculations, the ground-state atomic geometries were fully relaxed till the forces on the atoms smaller than 0.03 eV $Å^{-1}$.

## Results and discussion

Figure 1 shows a schematic illustration of fabrication process of S-CNTs/SiC composite. The XRD patterns of sulfur, CNTs/SiC, and S-CNTs/SiC composite are gathered in Fig. 2. Compared to sulfur, the characteristic peaks of sulfur can clearly be distinguished in the S-

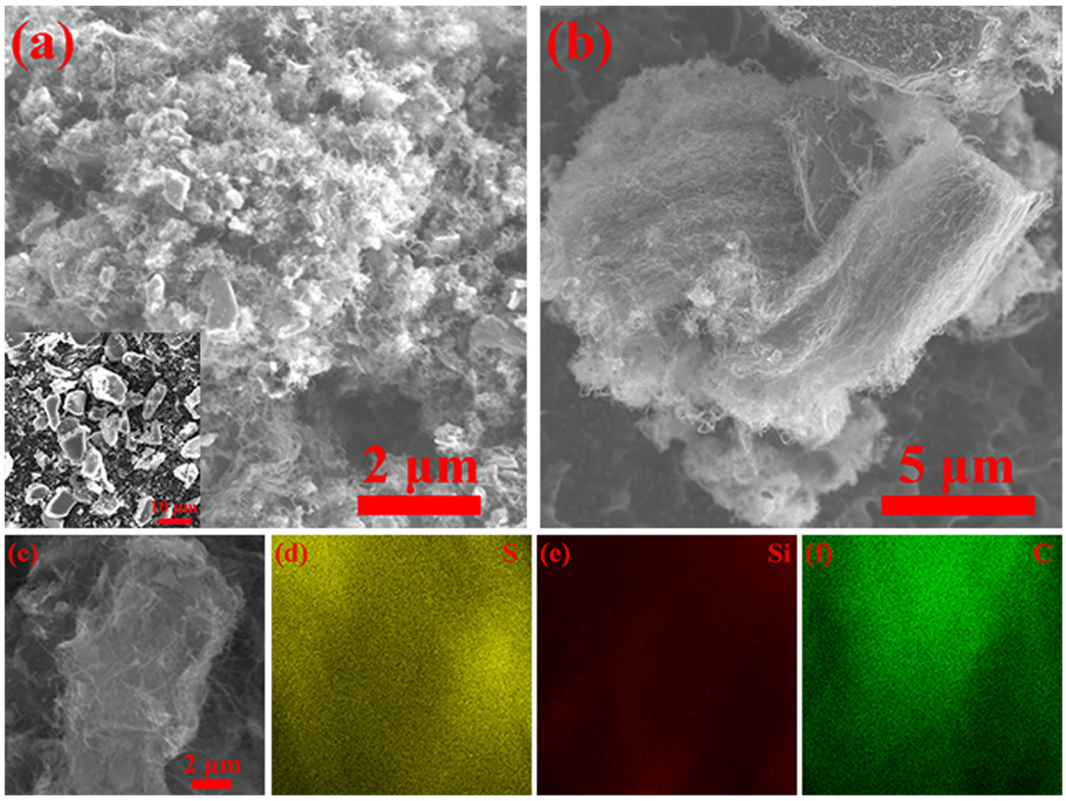


**Fig. 3** SEM images of **a**, **b** CNTs/SiC at different magnifications and pure SiC (inset of **a**), **c**, **d**, **e**, **f** S-CNTs/SiC and corresponding S, Si, and C mapping, respectively

CNTs/SiC spectra, indicating the successful loading of S on CNTs/SiC. The peaks of CNTs/SiC also suggested that introduction of sulfur did not change CNTs/SiC structure. No other impurity peaks were detected, confirming the high purity of the synthesized composites. Moreover, the characteristic peak intensity of S was much higher than those of CNTs and SiC, indicating that S content far exceeded those of CNTs and SiC. This was confirmed by TGA results with loading rate of S reaching 75.6% (Fig. 6).

Figure 3a, b clearly shows that surface of SiC was successfully loaded with carbon nanotubes, grown and entangles to form clusters. In turn, these clusters should play important role in sulfur loading and relieving volume expansion. Figure 3c depicts that the array structure still effectively retained after sulfur loading, consistent with TEM results of CNTs/SiC (Fig. 4a) and S-CNTs/SiC (Fig. 4c). The corresponding EDS mapping of S, Si, and C elements of S-CNTs/SiC is shown in Fig. 3d–f). Uniform distributions of sulfur in presence of SiC and

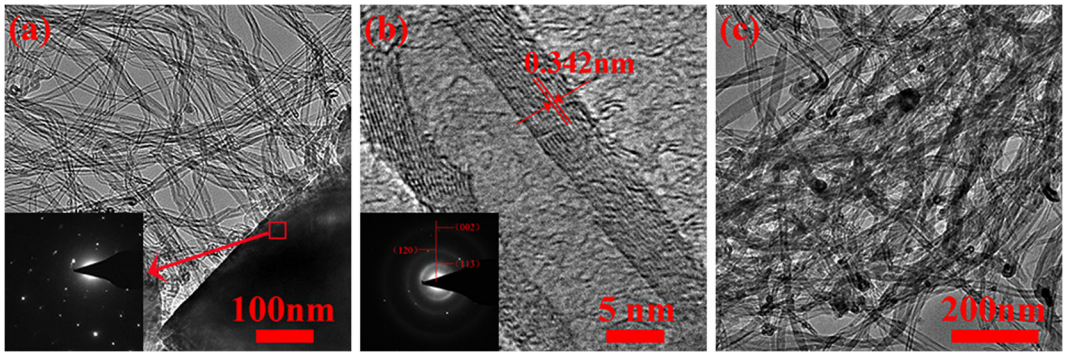


**Fig. 4** TEM images of **a** CNTs/SiC, **b** HRTEM image of CNTs, and **c** S-CNTs/SiC

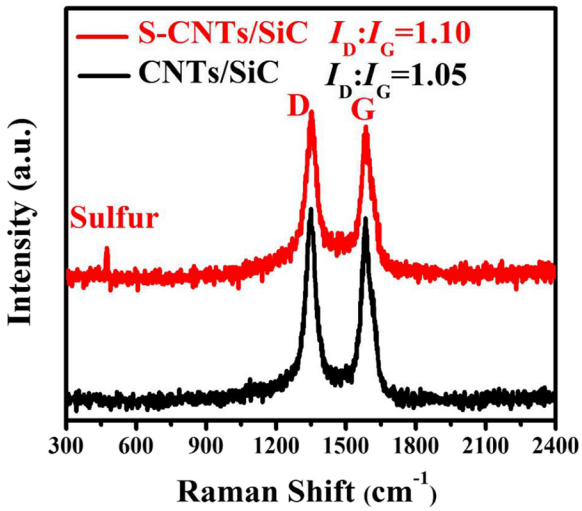


**Fig. 5** Raman spectra of CNTs/SiC and S-CNTs/SiC

CNTs were observed. Thus, carbon nanotubes certainly played a significant role in sulfur loading but Fig. 3d indicates that sulfur signal on SiC surface was stronger than that of CNTs. The latter should mainly be ascribed to strong Si–S interactions (Liu et al. 2016). The morphologies and structures of CNTs/SiC and S-CNTs/SiC were examined by TEM, and the results are depicted in Fig. 4. The tube wall looked clear with average diameter of approximately 10 nm (Fig. 4b); hence, sulfur can be stored in the tubes. The structures of carbon nanotube clusters are displayed in Fig. 4a, c. Their unique structures were advantageous for increasing sulfur loading. In other words, sulfur could not only be embedded in hollow carbon nanotubes but also stored in spaces between carbon nanotubes.

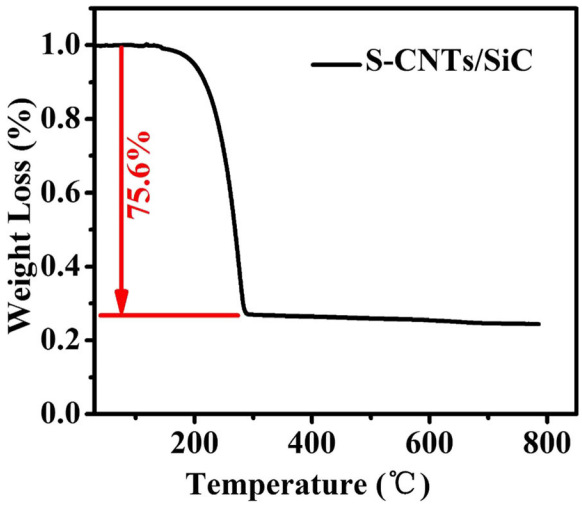


**Fig. 6** TGA analysis of S-CNTs/SiC

As shown in Fig. 5, the peaks of S-CNTs/SiC and CNTs/SiC appeared pretty similar, indicating that the process of sulfur loading process did not destroy CNTs/SiC structure. The two Raman bands at about 1330 cm$^{-1}$ (D band) and 1570 cm$^{-1}$ (G band) were associated with typical peaks of CNTs. The peak located at 460 cm$^{-1}$ can be attributed to sulfur. In addition, the $I_D/I_G$ ratio increased from 1.05 to 1.10, suggesting lower graphitization degree of S-CNTs/SiC when compared to CNTs/SiC. Hence, sulfur loading process increased defects in S-CNTs/SiC.

The sulfur content and thermal stability of S-CNTs/SiC composites were measured by TGA under argon atmosphere (Fig. 6). A main weight loss from 200 to 300 °C was noticed and attributed to evaporation of sulfur from S-CNTs/SiC composites. Such high weight loss (75.6%) indicated S-CNTs/SiC composites with great sulfur storage.

The surface structures were further identified by XPS analysis (Fig. 7). The surface of S-CNTs/SiC was composed of Si 2p, S 2p, C 1s, and O 1s. The corresponding peaks at binding energies of 164.3 eV, 164.6 eV, 165.4 eV, and 165.6 eV in high-resolution spectra of S 2p (Fig. 7b) were attributed to S–S, S–O, S–S, and S–O bond, respectively. The S–O bond may be caused by combination of S with oxygen-containing functional groups of carbon nanotubes and SiC. The bonds of Si–C and Si–O are detected at 100.9 eV and 104.0 eV in spectrum of Si 2p (Fig. 7c). The Si–O bond was associated with presence of residual $SiO_2$ on SiC surface. As shown in Fig. 6d, two peaks at 284.8 and 285.3 eV appeared and attributed to carbon nanotubes and oxygen-containing functional groups present on the surface. The specific surface of CNTs/SiC (61.63 m$^2$/g) and SiC (3.00 m$^2$/g) is performed in Fig. 8a. The CNT loading played a significant role in the increase of specific surface area, which can effectively immobilize LPS by physical adsorption. The presence of mesopores was simultaneously confirmed on the SiC and CNTs/SiC (Fig. 8b), while the number difference was significant. The small amount of mesopores on the surface of SiC can be attributed to the process of removing $SiO_2$ layers deposited on the commercial SiC surface by HF etching. And a large number of mesopores on the surface of CNTs/SiC were due to CNTs loaded on SiC.

The cycling performances for S-SiC and S-CNTs/SiC cathodes at current density of 0.1 C were investigated by galvanostatic charge-discharge method. After 100 cycles (Fig. 9a), the specific capacity of S-CNTs/

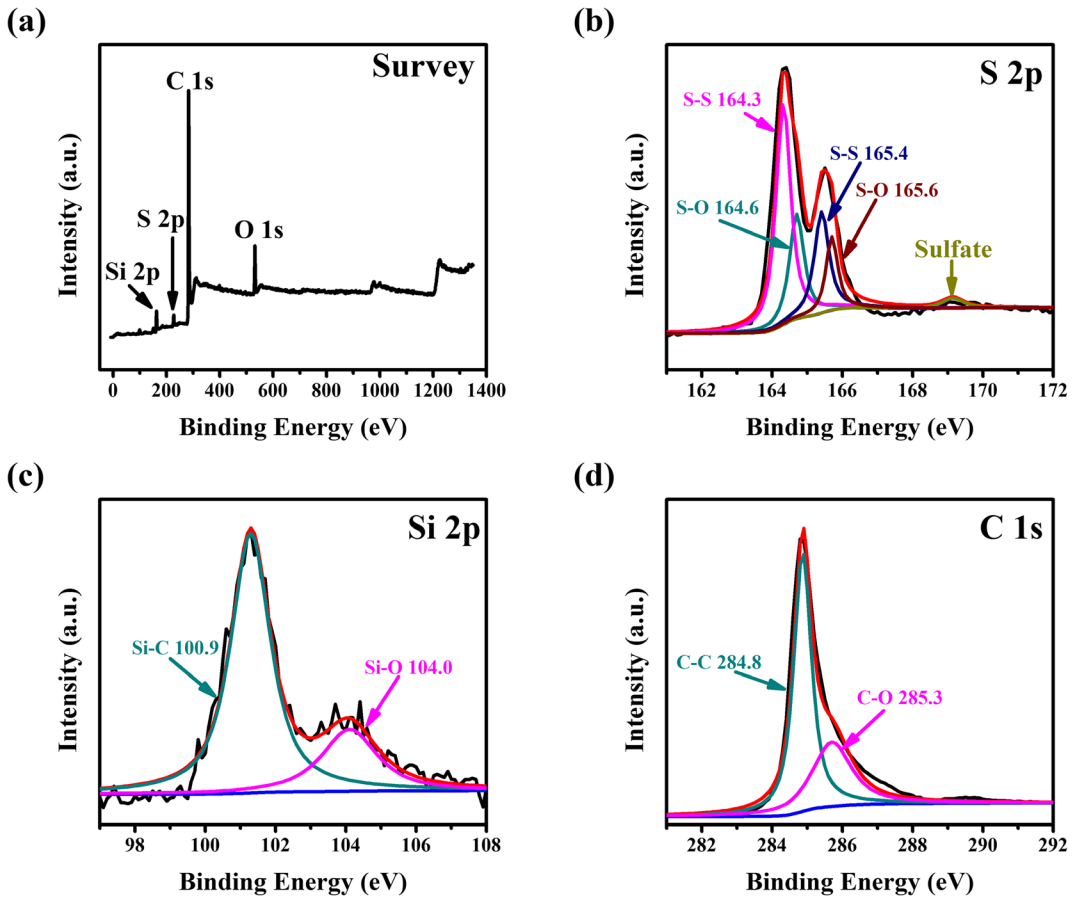


**Fig. 7** XPS spectra of S-CNTs/SiC composites: **a** wide spectrum and **b**, **c**, **d** high-resolution spectra of S 2p, Si 2p, and C 1s

SiC decreased from 1008 to 685 mAh $g^{-1}$ but obviously better than that of S-SiC. Even at a high current density of 1 C, the capacity of 316 mAh $g^{-1}$ can be maintained after 400 cycles (Fig. 9e). The improvements in electrical conductivity of the integrated composite through loading of carbon nanotubes increased transfer rates of

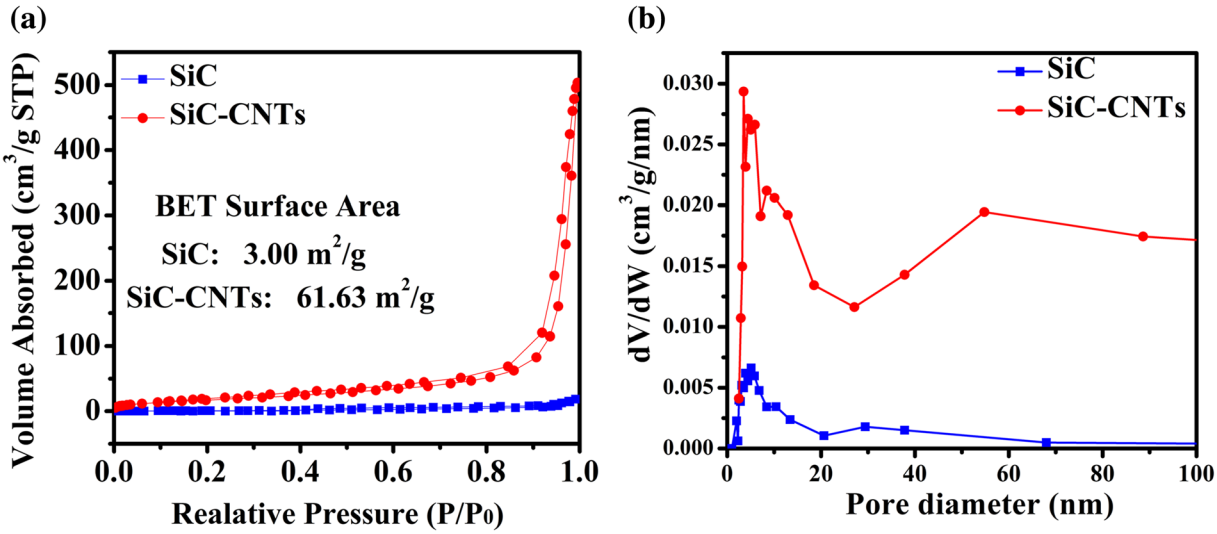


**Fig. 8** **a** $N_2$ ad-desorption isotherms and **b** pore size distribution of the SiC and CNTs/SiC

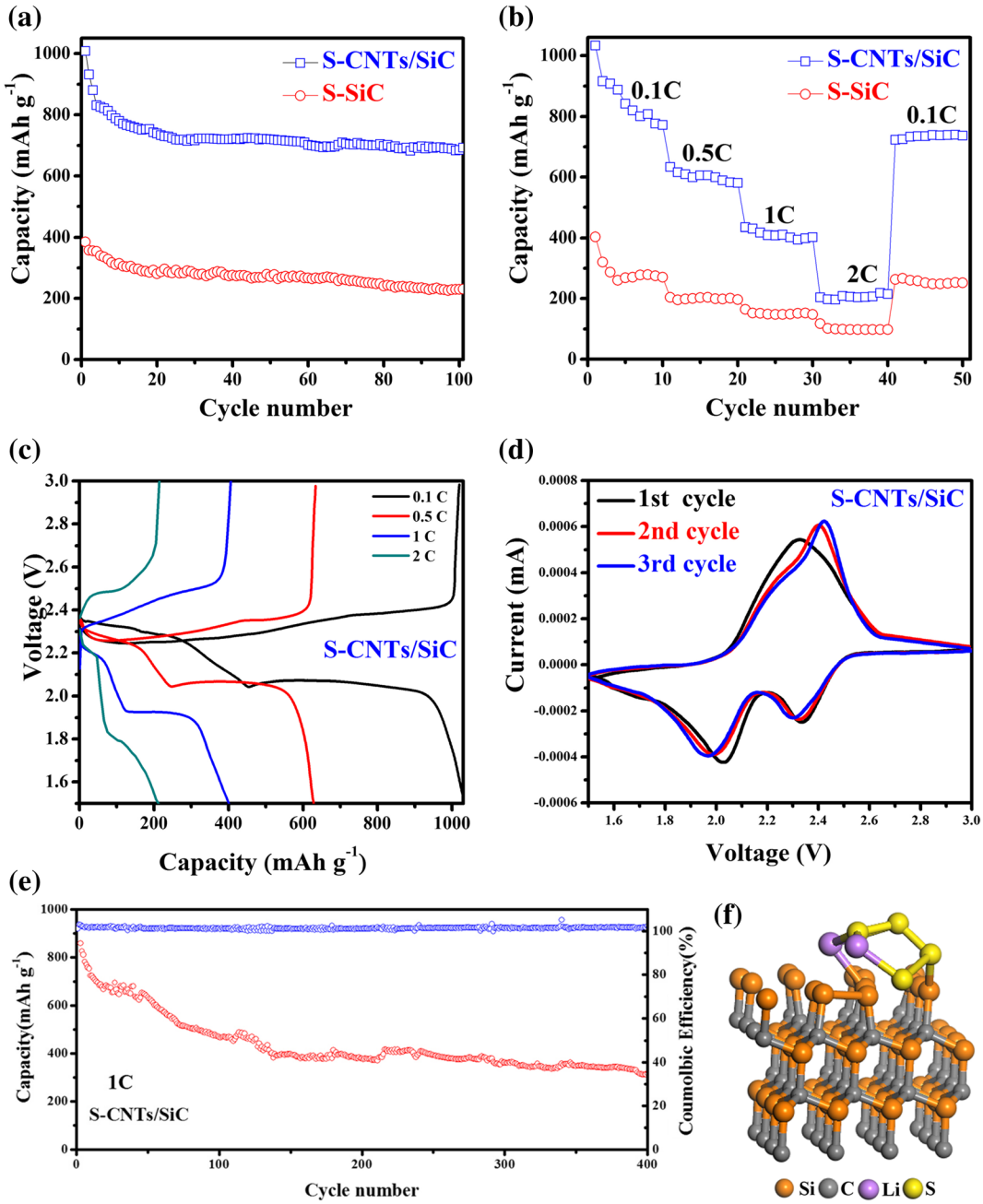


**Fig. 9** **a** Cycle performance of S-SiC and S-CNTs/SiC composites at 0.1 C, **b** rate capability of S-SiC and S-CNTs/SiC composite cathodes at various rates, **c** galvanostatic charge/discharge curves of S-CNTs/SiC composite at various rates, **d** CV curves of S-CNTs/SiC cathode at 0.1 mV $s^{-1}$ in the potential window from 1.5 to 3.0 V, **e** cycle performance of S-CNTs/SiC composites at 1 C, **f** adsorption configurations of $Li_2S_4$ on SiC (006) surface

electrons and lithium ions. This, in turn, induced higher utilization of active substances and significantly improved the capacity of S-CNTs/SiC cathode. The high cycling stability of S-CNTs/SiC would most likely be related to growth of carbon nanotubes on SiC matrix, greatly increasing loading of sulfur and adsorption of polysulfides during charge-discharge processes. Furthermore, the direct Si–S interaction obtained by SiC showed effective adsorption behavior of polysulfides, leading to high cycling stability (Li and Zhao 2018). To prove Si–S interaction obtained by SiC more intuitively, DFT calculation was implemented to investigate the

chemical adsorption effect of SiC on LPS. $Li_2S_4$ was employed as the representative LPS. As shown in Fig. 9f, adsorption configurations of $Li_2S_4$ on SiC (006) surface were displayed with a binding energy of 3.91 eV, implying direct Si–S interaction and strong confinement on LPS of SiC. At this point, the results of BET can be thought together. Ultra-low specific surface area (3.00 $m^2/g$) and a small amount of mesopores are displayed in Fig. 8a, b, which was almost impossible to physically adsorb LPS. It is worth noting that electrochemical performance of pure S-SiC electrode is described in Fig. 9a, b, low but stable specific capacities were demonstrated, meaning that LSB can work with S-SiC electrode. The possibility of physical adsorption was ruled out, the existence of Si–S bond by DFT calculation was proved; therefore, chemical adsorption (the presence of the Si–S bond) was used to explain why LSB can work with S-SiC electrode, which is considered reasonable and logical.

The rate performances of S-CNTs/SiC composites are presented in Fig. 9b, c. The current density increased stepwise from 0.1 to 2 C (1 C = 1675 mA $g^{-1}$) after every 10 successive cycles. Specific capacities of 1033, 572, 435, and 204 mAh $g^{-1}$ were delivered at 0.1, 0.5, 1, and 2 C rates, respectively. As current density decreased back to 0.1 C, the discharge capacity was maintained at 703 mAh $g^{-1}$, displaying relevant stability. The excellent electrochemical stabilities of S-CNTs/SiC electrodes were mainly due to effective adsorption to lithium polysulfides by combined physical adsorption of CNTs with chemical adsorption of SiC. Furthermore, the excellent effect in relieving volume changes of sulfur also played an important role in enhanced performances of LSBs. Though the capacity of S-SiC electrode was significantly lower than that of S-CNTs/SiC (Fig. 9b), excellent cycle stability was observed due to adsorption of SiC on lithium polysulfides caused by direct interaction between Si–S and Li–C (Li and Zhao 2018).

The galvanostatic discharge-charge curves (Fig. 9c) and CV (Fig. 9d) were used to identify the electrochemical reactions in S-CNTs/SiC electrode. The two reduction peaks at about 2.3 and 2.0 V were obtained. The peak at 2.3 V was attributed to reduction of $S_8$ to lithium polysulfides ($Li_2S_n$, $2 \le n \le 8$) and that at 2.0 V was assigned to transformation of lithium polysulfides to lithium sulfide ($Li_2S/Li_2S_2$). The peak at 2.4 V can be caused by transformation of lithium sulfides ($Li_2S/Li_2S_2$) into lithium polysulfides and sulfur (Zhu et al. 2016). The difference between the first and second cycle was due to possible structure rearrangement to more energetically stable sites, resulting in capacity fading over cycling.

## Conclusions

In sum, we synthesized S-CNTs/SiC composites by catalytic chemical vapor deposition then used as electrodes in LSBs with high sulfur loading of 75.6 wt%. The physical adsorption of carbon nanotubes and chemical adsorption SiC to polysulfides greatly reduced loss in active substances during cycling. DFT calculation was carried out to illustrate direct Si-S interaction and strong confinement on LPS of SiC. The S-CNTs/SiC electrodes delivered high specific capacities and cycling stabilities over cycles at 0.1 C and 1 C, respectively. Pure SiC electrode showed good cycle stability, confirming adsorption of SiC on lithium polysulfide. These findings demonstrated S-CNTs/SiC composite as promising candidate for LSBs.

**Funding information** Financial supports were received from the Natural Science Foundation of Hebei Province of China [grant no. E2015202037]; the Science and Technology Correspondent Project of Tianjin [grant no. 14JCTPJC00496]; Cultivation project of National Engineering Technology Center [grant no. 2017B090903008].

**Compliance with ethical standards** All relevant ethical standards were satisfied.

**Conflict of interest** The authors declare that they have no conflict of interest.

## References

Bao WZ, Zhang ZA, Chen W, Zhou CK, Lai YQ, Li J (2014) Facile synthesis of graphene oxide@mesoporous carbon hybrid nanocomposites for lithium sulfur battery. Electrochim Acta 127:342–348. https://doi.org/10.1016/j.electacta.2014.02.043

Bruce PG, Freunberger SA, Hardwick LJ, Tarascon JM (2012) Li-$O_2$ and Li–S batteries with high energy storage. Nat Mater 11:19–29. https://doi.org/10.1038/NMAT3191

Evers S, Yim T, Nazar LF (2012) Understanding the nature of absorption/adsorption in Nanoporous polysulfide sorbents for the Li–S battery. J Phys Chem C 116:19653–19658. https://doi.org/10.1021/jp304380j

He JR, Chen YF, Li PJ, Fu F, Wang ZG, Zhang WL (2015) Three-dimensional CNT/Graphene-sulfur hybrid sponges with high sulfur loading as superior-capacity cathode for Lithium-sulfur batteries. J Mater Chem A 3:18605–18610. https://doi.org/10.1039/C5TA04445F

He JR, Chen YF, Lv WQ, Wen KC, Wang ZG, Zhang WL, Li YR, Qin W, He WD (2016a) Three-dimensional hierarchical reduced Graphene oxide/tellurium nanowires: a high-performance free-standing cathode for Li−Te batteries. ACS Nano 10:8837–8842. https://doi.org/10.1021/acsnano.6b04622

He JR, Chen YF, Lv WQ, Wen KC, Xu C, Zhang WL, Li YR, Qin W, He WD (2016b) From metal−organic framework to $Li_2S$@C-co-N Nanoporous architecture: a high-capacity cathode for Lithium−sulfur batteries. ACS Nano 10:10981–10987. https://doi.org/10.1021/acsnano.6b05696

He JR, Lv WQ, Chen YF, Wen KC, Xu C, Zhang WL, Li YR, Qin W, He WD (2017a) Tellurium-impregnated porous cobalt-doped carbon Polyhedra as superior cathodes for Lithium −tellurium batteries. ACS Nano 11:8144–8152. https://doi.org/10.1021/acsnano.7b03057

He JR, Luo L, Chen YF, Manthiram A (2017b) Yolk–shelled C@$Fe_3O_4$ Nanoboxes as efficient sulfur hosts for high-performance Lithium–sulfur batteries. Adv Mater 29:1702707. https://doi.org/10.1002/adma.201702707

He JR, Chen YF, Manthiram A (2018a) Vertical $Co_9S_8$ hollow nanowall arrays grown on a Celgard separator as a multifunctional polysulfide barrier for high-performance Li–S batteries. Energy Environ Sci 11:2560–2568. https://doi.org/10.1039/c8ee00893k

He JR, Chen YF, Manthiram A (2018b) MOF-derived cobalt sulfide grown on 3D Graphene foam as an efficient sulfur host for long-life Lithium-sulfur batteries. iScience 4:36–43. https://doi.org/10.1016/j.isci.2018.05.005

He JR, Lv WQ, Chen YF, Xiong J, Wen KC, Xu C, Zhang WL, Li YR, Qin W, He WD (2018c) Direct impregnation of $SeS_2$ into MOFs-derived 3D Nanoporous co-N-C architecture towards superior rechargeable Lithium batteries. J Mater Chem A 6:10466–10473. https://doi.org/10.1039/C8TA02434K

He JR, Hartmann G, Lee M, Hwang GS, Chen YF, Manthiram A (2019) Freestanding 1T $MoS_2$/graphene heterostructures as a highly efficient electrocatalyst for lithium polysulfides in Li–S batteries. Energy Environ Sci 12:344–350. https://doi.org/10.1039/c8ee03252a

Hong XD, Liang J, Tang XN, Yang HC, Li F (2019) Hybrid graphene album with polysulfides adsorption layer for Li-S batteries. Chem Eng Sci 194:148–155. https://doi.org/10.1016/j.ces.2018.03.027

Hu YW, Liu XS, Zhang XP, Wan N, Pan D, Li XJ, Bai Y, Zhang WF (2016) Bead-curtain shaped SiC@$SiO_2$ core-shell nanowires with superior electrochemical properties for lithium-ion batteries. Electrochim Acta 190:33–39. https://doi.org/10.1016/j.electacta.2015.12.211

Huang JQ, Liu XF, Zhang Q, Chen CM, Zhao MQ, Zhang SM, Zhu WC, Qian WZ, Wei F (2013) Entrapment of sulfur in hierarchical porous graphene for lithium–sulfur batteries with high rate performance from −40 to 60 °C. Nano Energy 2:314–321. https://doi.org/10.1016/j.nanoen.2012.10.003

Ji XL, Lee KT, Nazar LF (2009) A highly ordered nanostructured carbon-Sulphur, cathode for lithium-Sulphur batteries. Nat Mater 8:500–506. https://doi.org/10.1038/nmat2460

Li Z, Jiang Y, Yuan LX, Yi ZQ, Wu C, Liu Y, Strasser P, Huang YH (2014) A highly ordered meso@microporous carbon-supported sulfur@smaller sulfur core-shell structured cathode for Li-S batteries. ACS Nano 8:9295–9303. https://doi.org/10.1021/nn503220h

Li F, Su Y, Zhao JJ (2016a) Shuttle inhibition by chemical adsorption of lithium polysulfides in B and N co-doped graphene for Li-S batteries. Phys Chem Chem Phys 18:25241–25248. https://doi.org/10.1039/c6cp04071c

Li F, Zhao JJ (2018) Three dimensional porous SiC for lithium polysulfide trapping. Phys Chem Chem Phys 20:4005–4011. https://doi.org/10.1039/c7cp07113b

Li HW, Yu HJ, Zhang XF, Guo GN, Hu JH, Dong AG, Yang D (2016b) Bowl-like 3C-SiC Nanoshells encapsulated in hollow graphitic carbon spheres for high-rate Lithium-ion batteries. Chem Mater 28:1179–1186. https://doi.org/10.1021/acs.chemmater.5b04750

Liu ZX, Balbuena PB, Mukherjee PP (2016) Evaluating silicene as a potential cathode host to immobilize polysulfides in lithium-sulfur batteries. J Coord Chem 11:1–33. https://doi.org/10.1080/00958972.2016.1184265

Miao LX, Wang WK, Wang AB, Yuan KG, Yang YS (2013) A high sulfur content composite with core–shell structure as cathode material for Li-S batteries. J Mater Chem A 1:11659–11664. https://doi.org/10.1039/C3TA12079A

Mikhaylik YV, Akridge JR (2004) Polysulfide shuttle study in the Li/S battery system. J Electrochem Soc 151:A1969–A1976. https://doi.org/10.1149/1.1806394

Wang HQ, Li S, Li D, Chen ZX, Liu HK, Guo ZP (2014) $TiO_2$ coated three-dimensional hierarchically ordered porous sulfur electrode for the lithium/sulfur rechargeable batteries. Energy 75:597–602. https://doi.org/10.1016/j.energy.2014.08.029

Wang SX, Zou KX, Qian YX, Deng YF, Zhang L, Chen GH (2018) Insight to the synergistic effect of N-doping level and pore structure on improving the electrochemical performance of sulfur/N-doped porous carbon cathode for Li-S batteries. Carbon 144:745–755. https://doi.org/10.1016/j.carbon.2018.12.113

Wei YY, Li X, Xu Z, Sun HY, Zheng YC, Li SP, Peng L, Li Z, Liu Z, Hu XZ, Zhao XL, Huang TQ, Zhao B, Xi JB, Gao C, Gao MX (2015) Solution Processible Hyperbranched inverse-vulcanized polymers as new cathode materials in Li-S batteries. Polym Chem 6:973–982. https://doi.org/10.1039/C4PY01055H

Wu DS, Shi FF, Zhou GM, Zu CX, Liu C, Liu K, Liu YY, Wang JY, Peng YC, Cui Y (2018) Quantitative investigation of polysulfide adsorption capability of candidate materials for Li-S batteries. Energy Storage Mater 13:241–246. https://doi.org/10.1016/j.ensm.2018.01.020

Xiang MW, Wu H, Liu H, Huang J, Zheng YF, Li Y, Jing P, Zhang Y, Dou SX, Liu HK (2017) Batteries: a flexible 3D multifunctional MgO-decorated carbon foam@CNTs hybrid as self-supported cathode for high-performance lithium-sulfur batteries. Adv Funct Mater 27:1702573. https://doi.org/10.1002/adfm.201702573

Yin FX, Liu XY, Zhang YG, Zhao Y, Menbayeva A, Bakenov Z, Wang X (2017) Well-dispersed sulfur anchored on interconnected polypyrrole nanofiber network as high performance cathode for lithium-sulfur batteries. Solid State Sci 66:44–49. https://doi.org/10.1016/j.solidstatesciences.2017.02.009

Zhang YG, Zhao Y, Konarov A, Gosselink D, Soboleski HG, Chen P (2013) A novel nano-sulfur/polypyrrole/graphene nanocomposite cathode with a dual-layered structure for lithium rechargeable batteries. J Power Sources 241:517–521. https://doi.org/10.1016/j.ssi.2013.03.006

Zhang YG, Zhao Y, Bakenov Z (2014a) A simple approach to synthesize nanosized sulfur/graphene oxide materials for high-performance lithium/sulfur batteries. Ionics 20:1047–1050. https://doi.org/10.1007/s11581-014-1165-5

Zhang YG, Zhao Y, Bakenov Z, Tuiyebayeva M, Konarov A, Chen P (2014b) Synthesis of hierarchical porous sulfur/polypyrrole/multiwalled carbon nanotube composite cathode for lithium batteries. Electrochim Acta 143:49–55. https://doi.org/10.1016/j.electacta.2014.07.148

Zhao Y, Wu WL, Li JX, Xu ZC, Guan LH (2014) Encapsulating MWNTs into hollow porous carbon nanotubes: a tube-in-tube carbon nanostructure for high-performance lithium-sulfur batteries. Adv Mater 26:5113–5118. https://doi.org/10.1002/adma.201401191

Zhou GM, Li L, Ma CQ, Wang SG, Shi Y, Koratkar N, Ren WC, Li F, Cheng HM (2015) A graphene foam electrode with high sulfur loading for flexible and high energy Li-S batteries. Nano Energy 11:356–365. https://doi.org/10.1016/j.nanoen.2014.11.025

Zhu FL, Yang Z, Zhao JP, Zhao X (2016) Microwave assisted preparation of expanded graphite/sulfur composites as cathodes for Li-S batteries. New Carbon Mater 31:199–204. https://doi.org/10.1016/S1872-5805(16)60011-2